RadioGraphics

MR Imaging: A "One-Stop Shop" Modality for Preoperative Evaluation of Potential Living Kidney Donors[1]

Shahid M. Hussain, MD, PhD • Marc C. J. M. Kock, MD
Jan N. M. IJzermans, MD, PhD • Peter M. T. Pattynama, MD, PhD
M. G. Myriam Hunink, MD, PhD • Gabriel P. Krestin, MD, PhD

CME FEATURE

See accompanying test at http://www.rsna.org/education/rg_cme.html

LEARNING OBJECTIVES

After reading this article and taking the test, the reader will be able to:

- Describe the varied anatomy of the renal vessels and collecting system.
- Discuss the basics of various MR imaging sequences and postprocessing methods used for preoperative evaluation of potential living kidney donors.
- List the advantages of a comprehensive MR imaging protocol over other modalities for evaluation of living kidney donors.

At many institutions, magnetic resonance (MR) angiography is the technique of choice for assessment of the renal arteries and renal parenchyma in potential living kidney donors. The renal arteries and renal veins have a varied anatomy and may consist of one or more vessels at several levels with variable calibers and levels of branching. These findings may play an important role in the surgeon's decision about which kidney to harvest, especially if laparoscopic nephrectomy is used. A comprehensive MR imaging protocol is used at one hospital to assess the arteries, veins, parenchyma, and collecting system of the kidneys. The protocol includes T2-weighted single-shot fast spin-echo imaging, fat-saturated T2-weighted fast spin-echo imaging, three-dimensional MR angiography and MR venography, and delayed fat-saturated three-dimensional T1-weighted gradient-echo imaging. Meticulous assessment of the source images as well as images produced with various postprocessing methods, such as full maximum intensity projection, targeted maximum intensity projection, and axial and oblique reformation, allows detailed description of the vascular anatomy and its relationship to the collecting system and parenchyma to facilitate the surgeon's decision making. The findings of MR imaging are comparable with those of other imaging modalities.

Abbreviations: DSA = digital subtraction angiography, GRE = gradient echo, IVC = inferior vena cava, MIP = maximum intensity projection, SE = spin echo, 3D = three-dimensional

Index terms: Kidney, MR, 81.1214 • Kidney, transplantation, 81.455 • Renal arteries, MR, 961.12942 • Renal veins, MR, 966.12942

RadioGraphics 2003; 23:505–520 • **Published online** 10.1148/rg.232025063

[1]From the Departments of Radiology (S.M.H., M.C.J.M.K., P.M.T.P., M.G.M.H., G.P.K.), Epidemiology and Biostatistics (M.C.J.M.K., M.G.M.H.), and Surgery (J.N.M.I.), Erasmus Medical Center, Dr Molewaterplein 40, 3015 GD Rotterdam, the Netherlands. Recipient of an Excellence in Design award for an education exhibit at the 2001 RSNA scientific assembly. Received March 21, 2002; revision requested May 2 and received June 24; accepted June 25. **Address correspondence to** S.M.H.

Introduction

With the prevalence of end-stage renal disease in the United States increasing at a rate of more than 8% per year and disparity between the donor supply and demand, the number of patients on waiting lists for kidney transplants has more than quadrupled during the past 2 decades (1,2). During the same period, the number of transplantations performed with cadaveric kidneys has remained unchanged or increased only slightly (1). Consequently, living donors have become increasingly important in kidney transplantation (1,2). Living donor transplantation helps reduce the prolonged waiting time for a cadaveric kidney and allows transplantation to be performed electively with a short cold-ischemia time (2). In addition, the recipients have better graft function and graft survival than following postmortem organ transplantation (2).

Laparoscopic nephrectomy is routinely performed at our institution. The laparoscopic method has lower morbidity, shorter hospitalization, more rapid convalescence, and a better cosmetic result (2). However, the laparoscopic method requires a longer surgical in-room time. In addition, in very obese patients and patients with bilateral complex renal vascular anatomy, the surgeons at our hospital prefer an open nephrectomy.

With the increasing reliance on living kidney donors in combination with laparoscopic nephrectomy, an accurate preoperative assessment of the donor is essential to minimize the risks for the donor and optimize the results for the recipient. The preoperative assessment includes an imaging work-up for complete evaluation of the arterial and venous anatomy, the collecting system, and the renal parenchyma (1). Failure to identify variations in the renal vasculature or collecting system or to detect parenchymal abnormalities may complicate the harvesting procedure as well as the transplantation procedure and may compromise the eventual outcome for the recipient (3).

Previously, digital subtraction angiography (DSA), intravenous urography, scintigraphy, and ultrasonography (US) were used in combination to visualize the anatomy and function of the renovascular and genitourinary systems (1). Recently, computed tomographic (CT) angiography and magnetic resonance (MR) angiography, which are less invasive than DSA, have been introduced as alternative techniques for the imaging work-up of living kidney donors (4–10). Reports from several centers mention replacement of DSA by CT angiography or MR angiography (9,10).

In this article, we describe our experience with a comprehensive MR imaging protocol and various methods for postprocessing in more than 50 living kidney donors. The findings of MR imaging are compared with those of other imaging modalities, such as US, intravenous urography, and DSA, to illustrate the ability of MR imaging to be a "one-stop shop" modality for preoperative assessment of living kidney donors.

MR Imaging Technique

For data acquisition, we use a 1.5-T system (Signa CV/i; GE Medical Systems, Milwaukee, Wis) with a torso phased-array coil. This is a dedicated cardiovascular system that is equipped with 40 mT/m high-performance gradients and ramp sampling capability for more efficient readouts. After explanation of the procedure and a brief interview to check for contraindications, an intravenous catheter (20 gauge) is placed into the antecubital fossa and connected to a power injector (Spectris; Medrad, Indianola, Pa). In addition, a respiratory sensor is positioned around the patient for any MR imaging sequences with respiratory gating.

At our institution, the MR imaging protocol used to assess living kidney donors includes the following sequences (Fig 1):

1. Coronal single-shot fast SE or half-Fourier single-shot turbo SE imaging with the following parameters: repetition time (msec)/echo time (msec), ∞/120; flip angle, 90°; and acquisition time, 20 seconds (breath hold). This heavily T2-weighted sequence provides an overview of the upper abdominal anatomy, renal parenchyma, and collecting system and serves as a localizing sequence for planning the other sequences in the protocol.

2. Sagittal single-shot fast SE or half-Fourier single-shot turbo SE imaging with the following parameters: ∞/100; flip angle, 90°; and acquisition time, 16–20 seconds (breath hold). This sequence shows the anterior and posterior contours of the kidneys as well as their relationship to the liver and spleen.

3. Axial T2-weighted fast SE imaging with fat saturation performed with the following parameters: 2,000/100; flip angle, 90°; and acquisition time, 2 minutes 36 seconds (respiratory triggering). This is a sequence with high contrast and spatial resolution for detection of any renal parenchymal abnormalities.

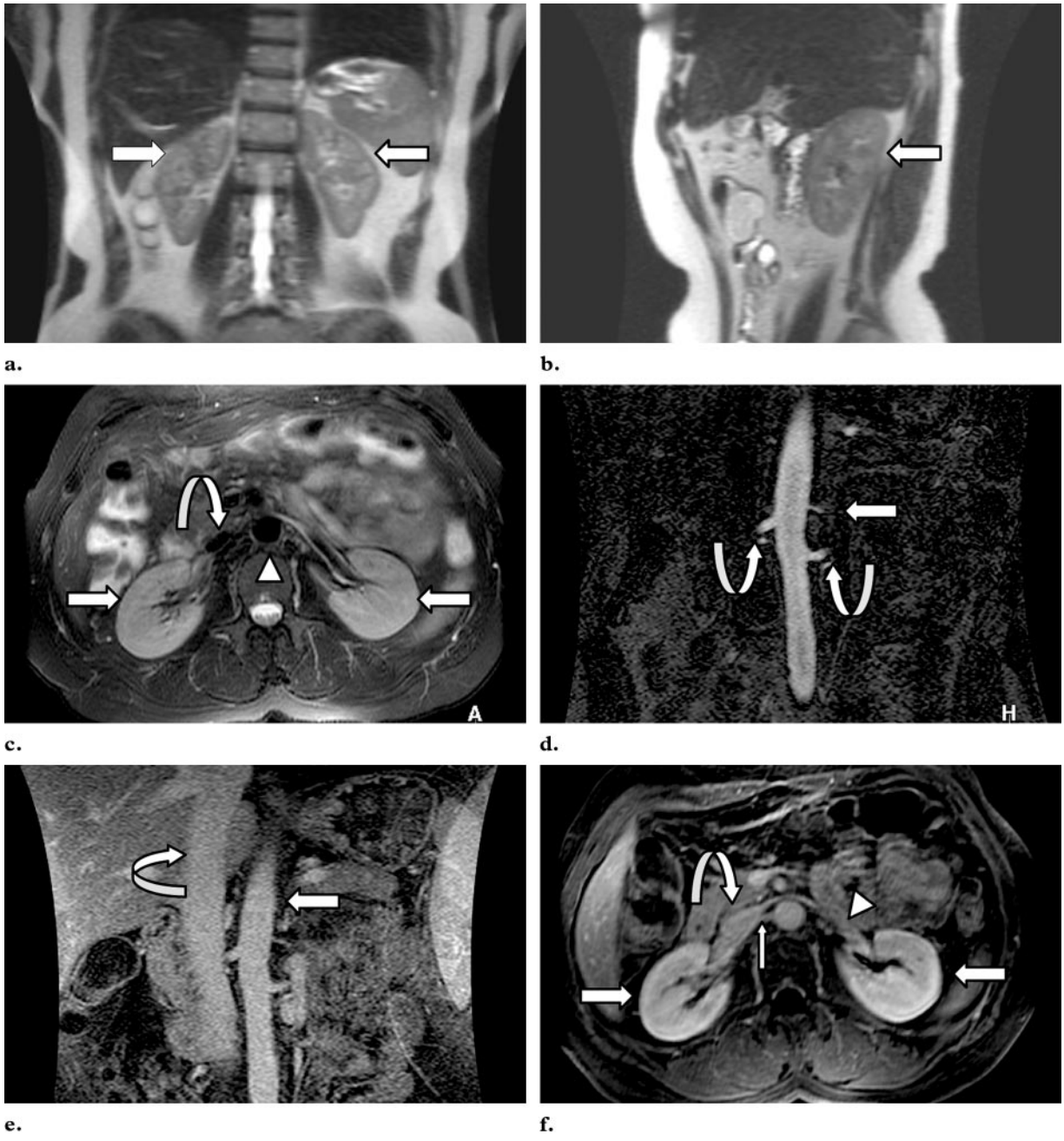

Figure 1. MR imaging protocol for evaluation of living kidney donors. **(a)** Coronal T2-weighted single-shot fast spin-echo (SE) or half-Fourier single-shot turbo SE image shows the kidneys (arrows), which have low signal intensity relative to their surroundings. This sequence allows simple and reproducible measurement of both kidneys. **(b)** Sagittal T2-weighted single-shot fast SE or half-Fourier single-shot turbo SE image shows the right kidney (arrow) in a different orientation. **(c)** Axial fat-saturated T2-weighted fast SE image shows both kidneys (straight arrows), which are hyperintense relative to their surroundings. Note the aorta (arrowhead) and inferior vena cava (IVC) (curved arrow), which demonstrate signal void due to flow compensation. **(d)** Coronal gadolinium-enhanced T1-weighted three-dimensional (3D) fast gradient-echo (GRE) source image shows the strongly enhanced aorta (straight arrow) and renal arteries (curved arrows). Before acquisition of this gadolinium-enhanced data set, an identical unenhanced sequence is performed to assess the patient's breath-holding ability and to obtain any subtraction images needed for postprocessing. **(e)** Coronal T1-weighted 3D fast GRE image obtained during the venous phase shows enhancement of the IVC (curved arrow) and aorta (straight arrow). **(f)** Axial delayed gadolinium-enhanced T1-weighted 3D fast GRE image obtained with fat saturation shows homogeneous enhancement of both kidneys (large straight arrows) and enhancement of the left renal vein (arrowhead) and IVC (curved arrow). Note that the right renal artery (small straight arrow) runs behind the IVC.

4. A timing bolus sequence performed with sagittal 3D fast GRE imaging with the following parameters: 4.2/1.8; flip angle, 70°; and acquisition time, one image per second for 60 seconds (free breathing). This sequence is performed after injection of exactly 2 mL of gadolinium contrast material with the power injector at a rate of 3 mL/sec. This is immediately followed by 15 mL of a saline flushing solution administered at a rate of 3 mL/sec. During imaging, the MR technologists observe the arrival of contrast material within the heart, thoracic aorta, and abdominal aorta. On the basis of this imaging data set, an imaging delay is calculated (see details later in this section).

5. Coronal 3D fast GRE MR angiography with the following parameters: 4.7/1.4; flip angle, 30°; 0.6 signal acquired; 256 × 192 × 24 matrix with a section thickness of 2.4 mm, zero-filled to 48 sections with overlapping reconstructed sections; and acquisition time, 24 seconds (breath hold). This sequence serves as the main MR angiography data set and is performed before and after the contrast material injection.

6. Coronal 3D fast GRE MR venography with the following parameters: 4.7/1.4; flip angle, 15°; 0.6 signal acquired; 256 × 192 × 24 matrix with a section thickness of 2.4 mm, zero-filled to 48 sections with overlapping reconstructed sections 1.2 mm thick; and acquisition time, 24 seconds (breath hold). This sequence is started as soon as possible after the MR angiography sequence. Usually, about 30–60 seconds will be needed to perform the prescanning and to adjust the imaging volume on the localizing image.

7. Axial delayed gadolinium-enhanced 3D fast GRE imaging with the following parameters: 4.9/1.6; flip angle, 15°; section thickness of 8 mm, zero-filled to 56 overlapping reconstructed sections 4 mm thick; and acquisition time, 21 seconds (breath hold). This sequence is used to confirm any parenchymal abnormalities that might have been present on the T2-weighted fast SE images with fat saturation.

This is a comprehensive MR imaging protocol for assessment of the renal parenchyma, renal arteries, renal veins, and renal collecting system. Before performance of the 3D MR angiography sequence, a single image from the timing bolus sequence is selected on the console and a region of interest is placed within the aorta at the level of the large abdominal vessels. On the basis of the region of interest, a time-intensity curve is generated. The time-intensity curve shows the time in seconds at which the peak enhancement of the arterial vessels is reached. On the basis of this time, the imaging delay for the main 3D gadolinium-enhanced MR angiography sequence can be calculated as follows: imaging delay = (contrast material arrival time) + (injection time/2) − (imaging time/2) (Fig 2). The 3D MR angiography sequence is performed after injection of 28 mL of gadopentetate dimeglumine (Magnevist; Schering, Berlin, Germany) with the power injector at a rate of 3 mL/sec. The contrast material injection is followed by 15 mL of saline flushing solution.

To depict the arteries and veins, we use two slightly different sequences. For venous series, the flip angle is decreased and the sequence is performed after the MR angiography sequence. In general, the tissue contrast with a GRE sequence can be influenced by changing the values of the repetition time, echo time, and flip angle. By using minimum values of repetition time and echo time, as we do for the MR angiography and MR venography sequences at our institution, the tissue contrast will mainly be influenced by the flip angle. In the MR angiography sequence, the focus is on the T1-shortening effect of gadopentetate dimeglumine within the arteries, and the signal from the background tissue is minimized. Both of these effects are achieved by choosing a relatively high value of the flip angle (approximately 40°). Decreasing the flip angle, for instance to a value of 15° as we do for the MR venography sequence, will generate more background tissue signal. In our opinion, a lower value of the flip angle in the MR venography sequence is necessary to compensate for the dilution of the gadopentetate dimeglumine that naturally takes

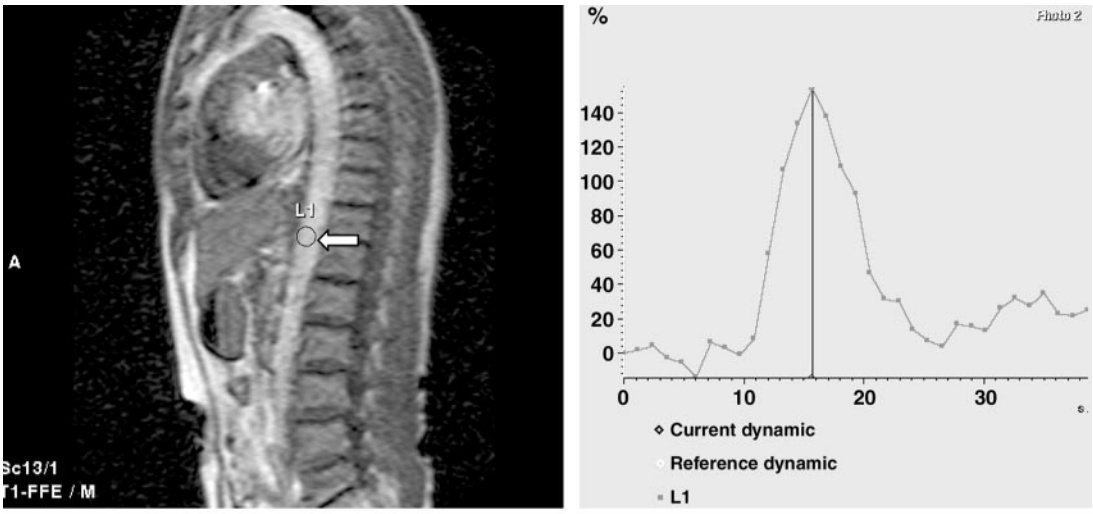

a. b.

Figure 2. Timing bolus sequence. **(a)** Sagittal T1-weighted two-dimensional fast field echo image (free breathing) with a section thickness of 2 cm shows the aorta. To capture the peak enhancement of the aorta, approximately 40–50 images are acquired at a temporal resolution of about two images per second. This temporal resolution allows the operator to actually see the arrival of the contrast medium within the heart, thoracic aorta, and abdominal aorta. Imaging is stopped after about 25 seconds or continued till the peak enhancement of the abdominal aorta has been satisfactorily observed. Note the region of interest at the level of the large abdominal vessels (arrow). **(b)** Time-intensity curve generated from the region of interest in **a** shows that the peak enhancement of the aorta at the level of the large abdominal vessels occurs at 15.7 seconds. On the basis of this value, the imaging delay for the main 3D gadolinium-enhanced MR angiography sequence can be calculated as follows: imaging delay = (contrast material arrival time) + (injection time/2) − (imaging time/2).

place because of the recirculation of the contrast medium within the vascular system as well as its excretion by the kidneys (3).

In our experience, a frequency and phase matrix of 256 × 192 in combination with the overlapping reconstructed sections in the MR angiography sequence yielded sufficient in-plane resolution to depict the relatively small arteries within a relatively short breath-hold time. Increasing the frequency matrix, for instance to 512, would decrease the signal-to-noise ratio, and increasing the phase matrix would increase the imaging time in such a fashion that fewer patients would be able to perform breath holding during data acquisition. The MR angiography and MR venography sequences are coronal oblique series that are angulated parallel to the abdominal aorta, particularly at the level of the kidneys. The venous anatomy can also be appreciated with the axial delayed gadolinium-enhanced sequence. The latter sequence, in combination with the fat-saturated T2-weighted fast SE sequence, is also important for visualization of the anterior and posterior contours of both kidneys as well as for assessment of any parenchymal abnormalities (3). These contours of the kidneys may not be imaged well with the coronal 3D MR angiography and MR venography sequences because these sequences are optimized to cover the vasculature of the kidneys with a minimum number of partitions in the y direction that can be acquired within a comfortable breath hold. The entire protocol takes about 30–40 minutes.

Postprocessing of 3D Data Sets

After completion of all MR imaging sequences, results of the entire examination are digitally transported to a workstation (Advantage Windows [GE Medical Systems] or EasyVision [Philips Medical Systems, Best, the Netherlands]). On

Figure 3. Postprocessing of an MR angiography data set from a living kidney donor. **(a)** Coronal full maximum intensity projection (MIP) image shows the aorta and its tributaries, including the main renal arteries (curved arrows), accessory renal arteries (straight arrows), and lumber arteries (arrowhead). **(b)** Coronal oblique linear reformatted image angled along the approximate course of the right renal vessels shows the main renal artery (curved arrow) and accessory renal artery (straight arrow) more clearly. **(c)** Coronal oblique linear reformatted image angled along the course of the left renal vessels shows the main renal artery (curved arrow), accessory renal artery (straight arrow), and lumber artery (arrowhead) more clearly. **(d)** Coronal targeted MIP image obtained at the origin of the renal arteries shows the relationship between the main renal arteries (curved arrows) and accessory renal arteries (straight arrows) and the lumber arteries (arrowhead). **(e)** Axial reformatted image clearly shows the main renal arteries (curved arrow) and accessory renal arteries (straight arrow) originating from the aorta. **(f)** Axial reformatted image obtained at a different level clearly shows the relationship between the renal artery (curved arrow) and the lumber artery (arrowhead).

the workstation, the 3D MR angiography and MR venography data sets are used for the following postprocessing series (Fig 3):

1. Full MIP reconstruction: With this algorithm, the pixels with a maximum intensity level are selected to produce 3D reconstructed images of the entire data set. In the case of kidney donors, all source images from the MR angiography

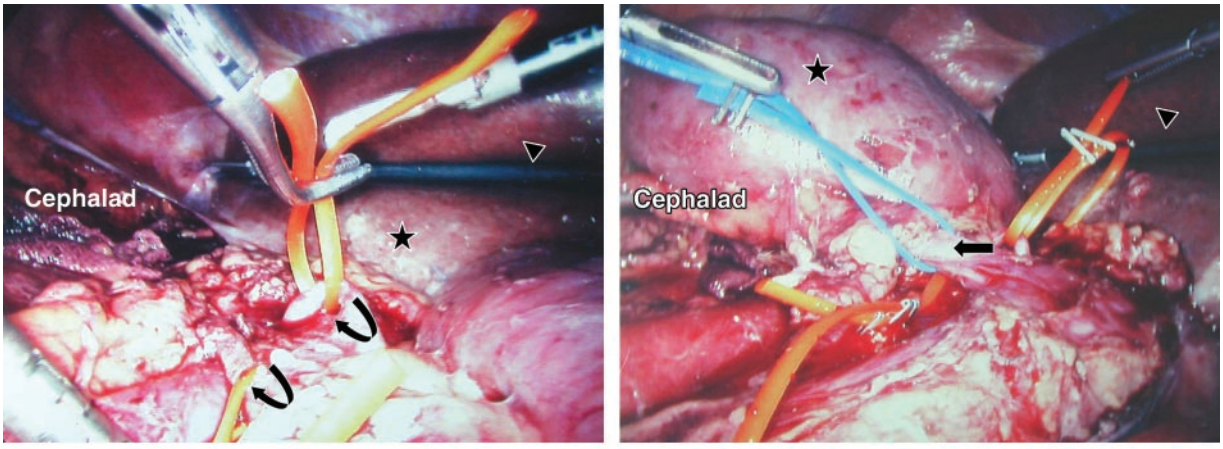

a. b.

Figure 4. Laparoscopic nephrectomy on the right side. *Cephalad* = cephalic aspect of the patient. **(a)** Photograph shows that two renal arteries (arrows) have been identified. The kidney (★) is still in situ, whereas the liver (arrowhead) has been pushed away slightly for better access to the kidney and its vessels. The left side of the patient is contiguous to the operating table. This position provides the surgeon with full access to the right flank. **(b)** Photograph shows that one renal vein (arrow) has been identified. The kidney (★) has been mobilized after dissection from the Gerota fascia and has been flipped over to the left side of the patient for better visualization of the renal vessels. Arrowhead = liver.

and MR venography data sets are used to provide an overview of the anatomy. The full MIP images can be reformatted along different angles and rotated in such a way that the vascular anatomy can be observed from different viewpoints (Fig 3a). The disadvantage of full MIP reconstruction is that the vessels that have enhanced to a certain level of intensity due to the presence of gadolinium will be displayed at the same time. This may hamper evaluation of the renal vessels. In addition, the distinction between the smaller accessory renal vessels and the lumber vessels may be difficult to appreciate on full MIP reconstructed images.

2. Partial or targeted MIP reconstruction: With this option, the user can select a certain number of source images or a certain part of the 3D data set to generate MIP reconstructed images. Targeted MIP reconstruction allows assessment of the vessels of interest without concurrent overprojection of other vessels. Often, we perform a number of targeted MIP reconstructions with variable thickness to cover the entire data set.

3. Coronal oblique, axial, and radial reformation: Owing to the almost isotropic nature of the 3D data sets, the source images can be reformatted in any desired plane or orientation. The spatial resolution of the reformatted images may be somewhat compromised compared with that of the source images because of some anisotropy as well as minimal artifacts that might be present due to the presence of pulsations and flow within the vessels, bowel peristalsis, and magnetic field inhomogeneity. Despite these limitations, in our experience the image quality with our set of parameters for the 3D MR angiography and MR venography sequences is fairly good in terms of providing the necessary diagnostic information concerning the relationship of the renal vessels to other surrounding vessels or organs. In particular, coronal oblique reformatted images obtained parallel to the right and left renal vessels provide detailed views of the origin as well as the entire course of the vessels (Fig 3). Radial reformatted images, which are obtained by using the aorta or the IVC at the level of the renal vessels as the center, often provide similar information as the coronal oblique reformatted images. Axial reformatted images are especially useful for assessing the relationship between the renal and lumber vessels.

4. Surface shading or fly-through rendering: These algorithms, although available on our workstations, are not routinely performed for evaluation of living kidney donors, mainly because such rendering can be time-consuming and its added value for assessment of living kidney donors is as yet uncertain.

MR Imaging Findings versus Those of Other Imaging Modalities

During the kidney harvesting procedure, and especially during laparoscopic nephrectomy, the surgeon will have limited access to the kidney and renal vessels (Fig 4). Because of frequent anatomic variability, the surgeon identifies the arteries, veins, and collecting system by careful dissection using the laparoscopic instruments. Any

a. b.

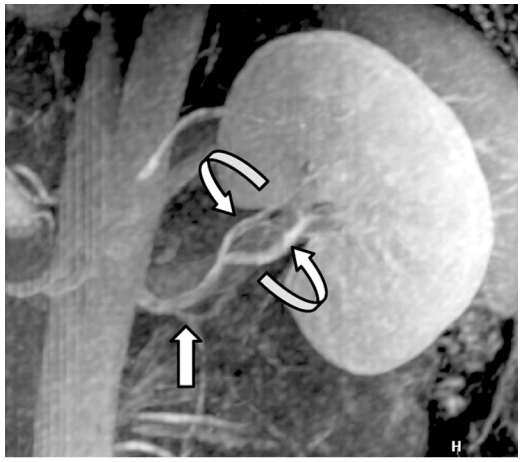

c.

Figure 5. Single renal artery and renal vein bilaterally with DSA–MR angiographic correlation. **(a)** DSA image shows the abdominal aorta and its tributaries, including the renal arteries (straight arrows). Note the branching of the left renal artery (curved arrows). **(b)** Coronal oblique reformatted image from the MR angiography data set shows one artery on the right side (straight arrow), one renal vein (curved arrow), and the enhanced renal pelvis (top arrowhead) with the proximal ureter (bottom arrowhead). **(c)** Coronal oblique reformatted image of the left side shows one renal artery (straight arrow) with branching (curved arrows). Note that the smaller intrarenal vessels are not seen on the MR angiograms **(b, c)**, in contrast to the DSA image **(a)**.

abrupt manipulation of vessels (eg, due to an unexpected anatomic variant) may result in conversion of the laparoscopic procedure into an open procedure or unmanageable bleeding.

Therefore, at our institution, results of all MR imaging examinations of living kidney donors, including the source images as well as all reconstructed images, are meticulously reviewed to determine the number of renal arteries, ascertain the number of renal veins and their anatomic position relative to other vessels, measure the length of the main renal artery to any parenchymal branching, exclude any vascular abnormalities, and assess the renal parenchyma (5). In our experience, MR imaging provides valuable information that is quite comparable to that of other imaging modalities, such as US, intravenous urography, and DSA. At our hospital, CT angiography is currently not performed in living kidney donors.

Variations in the number of renal arteries and in their position with respect to the renal veins are common. Vascular anatomic variations result from persistence of embryonic vessels that normally disappear when the definitive renal vessels form (11). Approximately 70% of the general population has single renal arteries bilaterally (4) (Fig 5). Extrahilar branching is a variant in which the main renal artery branches prior to reaching

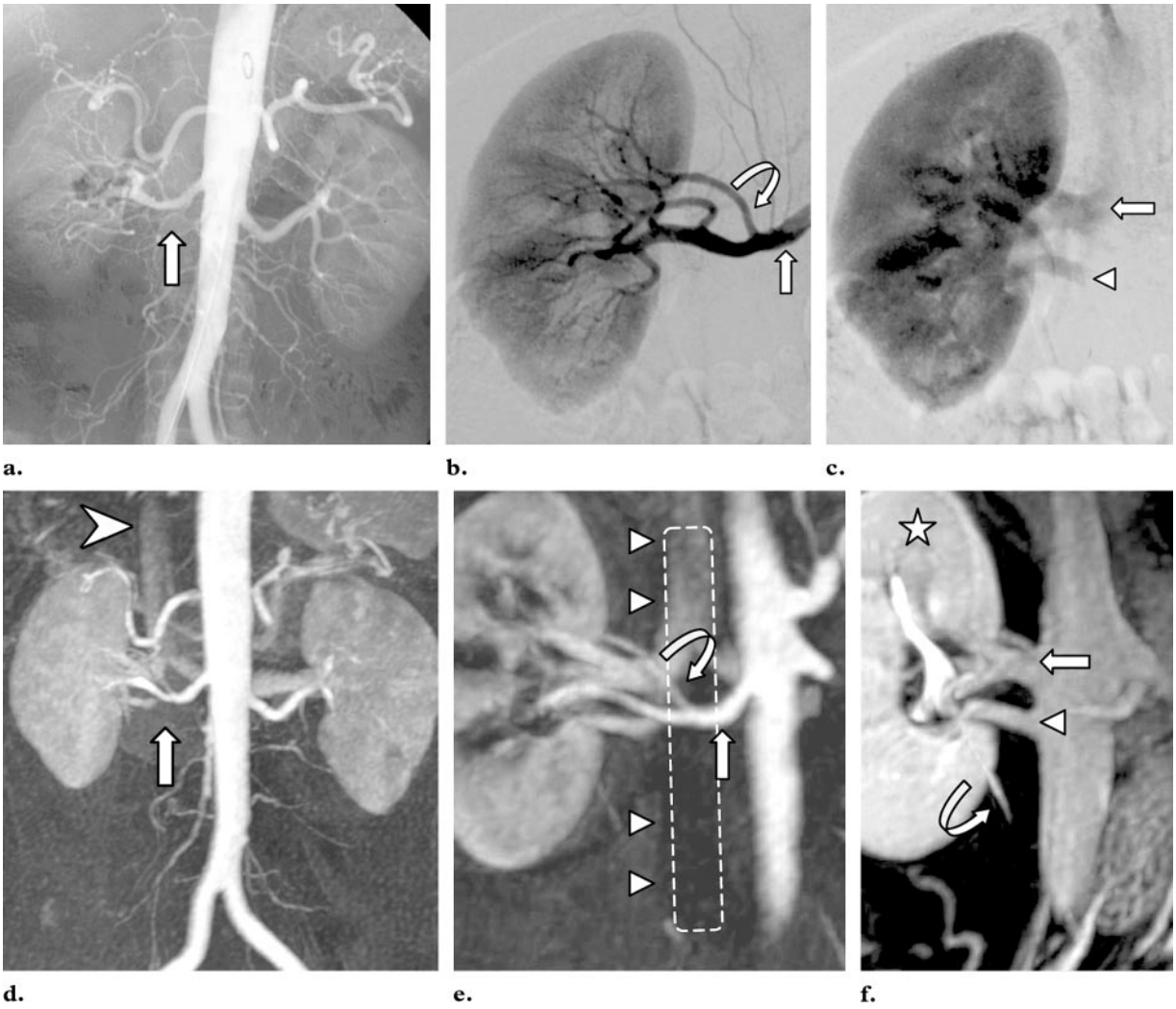

Figure 6. Early branching of the right renal artery and two right renal veins with DSA–MR angiographic correlation. **(a)** DSA image shows the abdominal aorta and its tributaries, including the right renal artery (arrow). **(b)** Selective DSA image of the right renal artery shows the main artery (straight arrow) and the first large branch (curved arrow), as well as some additional smaller branches distally. **(c)** Selective DSA image of the right kidney obtained during the venous phase shows slight enhancement of a large renal vein (arrow) and a small renal vein (arrowhead). **(d)** Coronal full MIP image from the MR angiography data set shows the aorta and its tributaries, including the right renal artery (arrow). Note the slight enhancement of the renal veins and part of the IVC (arrowhead) in this phase. **(e)** Coronal oblique reformatted image from the MR angiography data set shows the main right renal artery (straight arrow) and the first large branch (curved arrow). More distal smaller branches are not well visualized. The anatomic course of the IVC is indicated by a rectangular overlay (arrowheads). On the basis of the imaging findings, there seems to be sufficient distance between the origin of the renal artery and its first branch (about 2 cm). Therefore, the radiology report may suggest one renal artery on the right side. However, as the IVC runs anterior to the renal artery, the surgeon will not have access to the proximal part of the artery; therefore, from the surgical perspective, three arteries are present on the right. **(f)** Coronal oblique reformatted image of the venous phase clearly shows the large (straight arrow) and small (arrowhead) right renal veins originating from the IVC. Note also the homogeneous enhancement of the kidney (☆) and the renal pelvis and proximal ureter (curved arrow).

the renal parenchyma (4) (Figs 5–7). Arbitrarily, the surgeon will consider any branching within 1.5–2 cm, measured from the origin of the vessel with the aorta, as two separate vessels (4,7). This is mainly based on practical reasons because the surgeon will need a certain length to clamp the vessels before ligation.

Figure 7. Relationship between the renal arteries, IVC, renal veins, and collecting systems. **(a)** Coronal full MIP image from the MR angiography data set shows one renal artery on the left side (top straight arrow) and branching of the right renal artery (bottom straight arrow) into three tributaries (arrowheads). Note the lumber artery (curved arrow). **(b)** Coronal targeted MIP image of the venous phase shows the complex relationship between the renal arteries (straight arrows), renal veins (curved arrows), and collecting systems (arrowheads). Note that the IVC is anterior to the right renal artery; thus, the IVC covers the origin of this artery as well as the proximal parts of its branches (which are shown in **a**). Note also that the renal vein on the left side (dotted lines) is much longer than that on the right. **(c)** Coronal targeted MIP image of the venous phase obtained slightly posterior clearly shows the collecting systems, including the renal pelves (arrowheads) and proximal ureters (arrows). At this level, the vertebrae *(V)* with their vessels are visible.

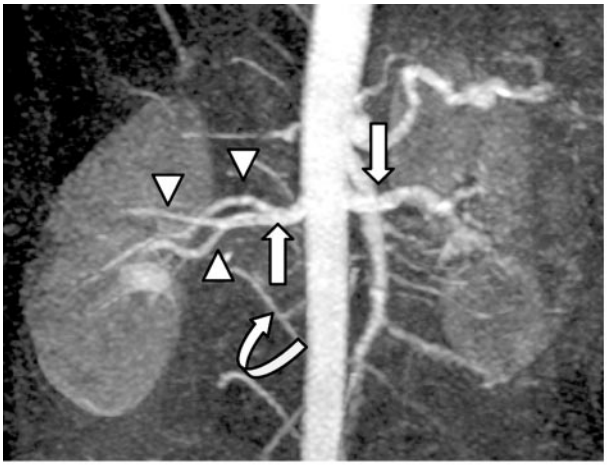

a.

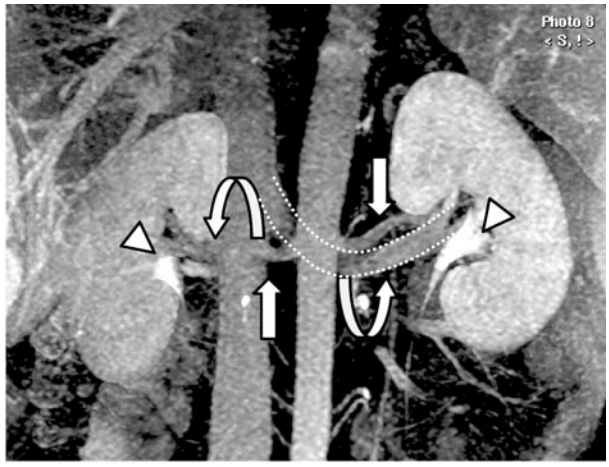

b.

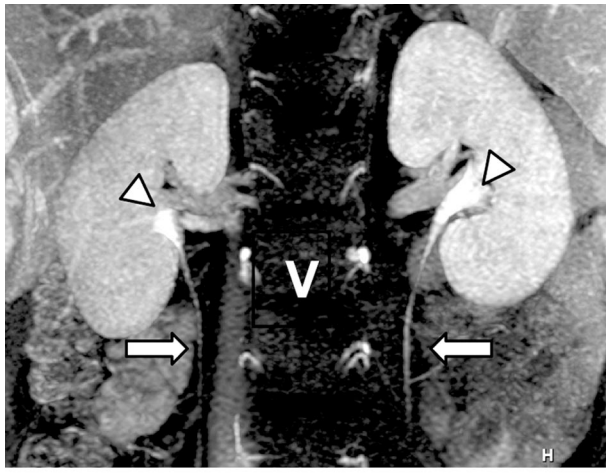

c.

During laparoscopic nephrectomy of the right kidney, the same distance should be measured from the lateral aspect of the IVC. The artery on the right side usually runs posterior to the renal vein and the IVC (Fig 1f). To avoid any damage, the renal arteries on the right side are clamped at a safe distance from the IVC. Therefore, if a laparoscopic nephrectomy is considered, it is essential to describe the exact relationship between the (branching) arteries and the IVC to the surgeon because the extent to which the vessels can be manipulated during the laparoscopic procedure is relatively limited. The ability of the surgeon to clamp the vessels will depend on the distance and the number of branches between the lateral margin of the IVC and the hilum of the right kidney. Failure to describe the exact findings may unnecessarily lengthen the procedure or complicate it with life-threatening bleeding. In the latter case, conversion to an open procedure will be inevitable.

According to the classic anatomy literature, about 20%–30% of kidneys have two or more arteries (Fig 8), and multiple vascular supply by more than three vessels to one kidney is possible (11). In recent studies of living kidney donors with CT angiography and MR angiography, accessory arteries were found in 40%–46% of cases

Figure 8. Two renal arteries bilaterally with DSA–MR angiographic correlation. **(a)** DSA image shows two renal arteries on the left side (straight arrows) and two renal arteries on the right (arrowheads). Curved arrow = superior mesenteric artery. **(b)** Coronal full MIP image from the MR angiography data set obtained with a slight rotation to the right shows the right renal arteries (arrowheads) with overprojection of the superior mesenteric artery (curved arrow). Conversely, on the left side, the entire course of both arteries (straight arrows) can be seen without overprojection. **(c)** Coronal oblique reformatted image from the MR angiography data set obtained parallel to the course of the right renal vessels clearly shows the renal arteries (arrowheads) originating from the aorta and entering the right kidney. On the left side, the origins of both renal arteries are visible (arrows).

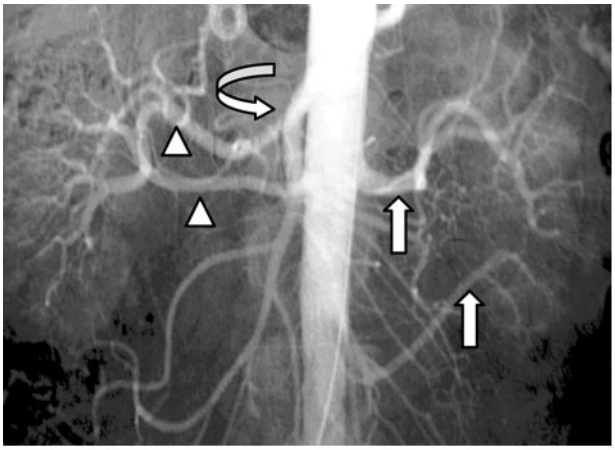

a.

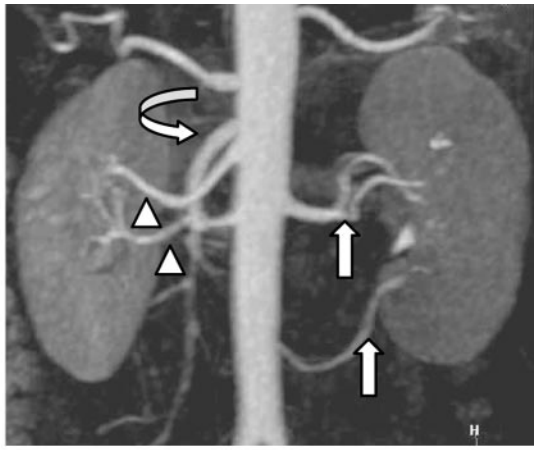

b.

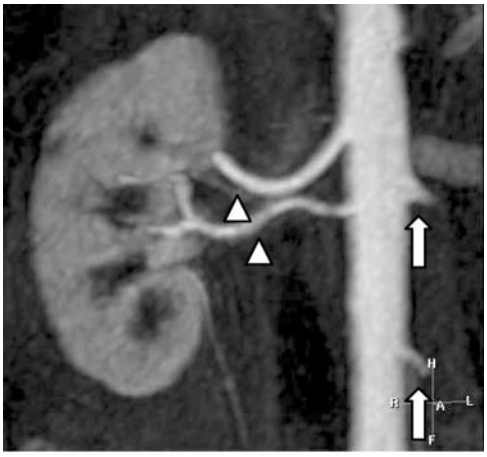

c.

(4,5,7). Supernumerary arteries, usually two or three, are twice as common as supernumerary veins (11). About 85% of the population has a single right renal vein, often without any tributary veins from other organs or structures (Fig 5) (4). This is the main reason why the right kidney is preferred for laparoscopic nephrectomy at our institution. However, the renal vein on the right side is much shorter than that on the left.

Similarly to the renal arteries, the renal veins may show a number of variations in anatomy, branching of the main renal vein, accessory veins, retroaortic veins, and circumaortic veins (Figs 6, 9). The anatomy of the left renal vein and its tributaries is often very complex. The most common variant of the left renal vein is a circumaortic configuration, which occurs in about 5%–7% of cases (Fig 9) (4). A single retroaortic left renal vein can be seen in 2%–3% of individuals (4). In addition to its own anatomic variability, the left renal vein has numerous tributaries, including the

Figure 9. Circumaortic left renal vein. **(a)** Coronal full MIP image from the MR angiography data set shows one renal artery bilaterally (arrows). **(b)** Coronal targeted MIP image of the venous phase shows the superior leg of a circumaortic left renal vein (curved arrow) draining into the IVC (straight arrow). **(c)** Coronal targeted MIP image of the venous phase obtained slightly posterior shows the inferior leg of the circumaortic renal vein (curved arrow) draining into the IVC (straight arrow). **(d)** Axial delayed gadolinium-enhanced 3D fast GRE image obtained with fat saturation at the level of the midpoles of the kidneys (arrowheads) shows the superior leg of the circumaortic renal vein (curved arrow) draining into the IVC (straight arrow). **(e)** Axial delayed gadolinium-enhanced 3D fast GRE image obtained with fat saturation at the level of the lower poles of the kidneys (arrowheads) shows the inferior leg of the circumaortic renal vein (curved arrow) crossing behind the aorta and draining into the IVC (straight arrow). **(f)** Axial single-shot fast SE image obtained at the level of the lower poles of the kidneys (arrowheads) shows the inferior leg of the circumaortic renal vein (curved arrow), which appears as an area of signal void, crossing behind the aorta and draining into the IVC (straight arrow).

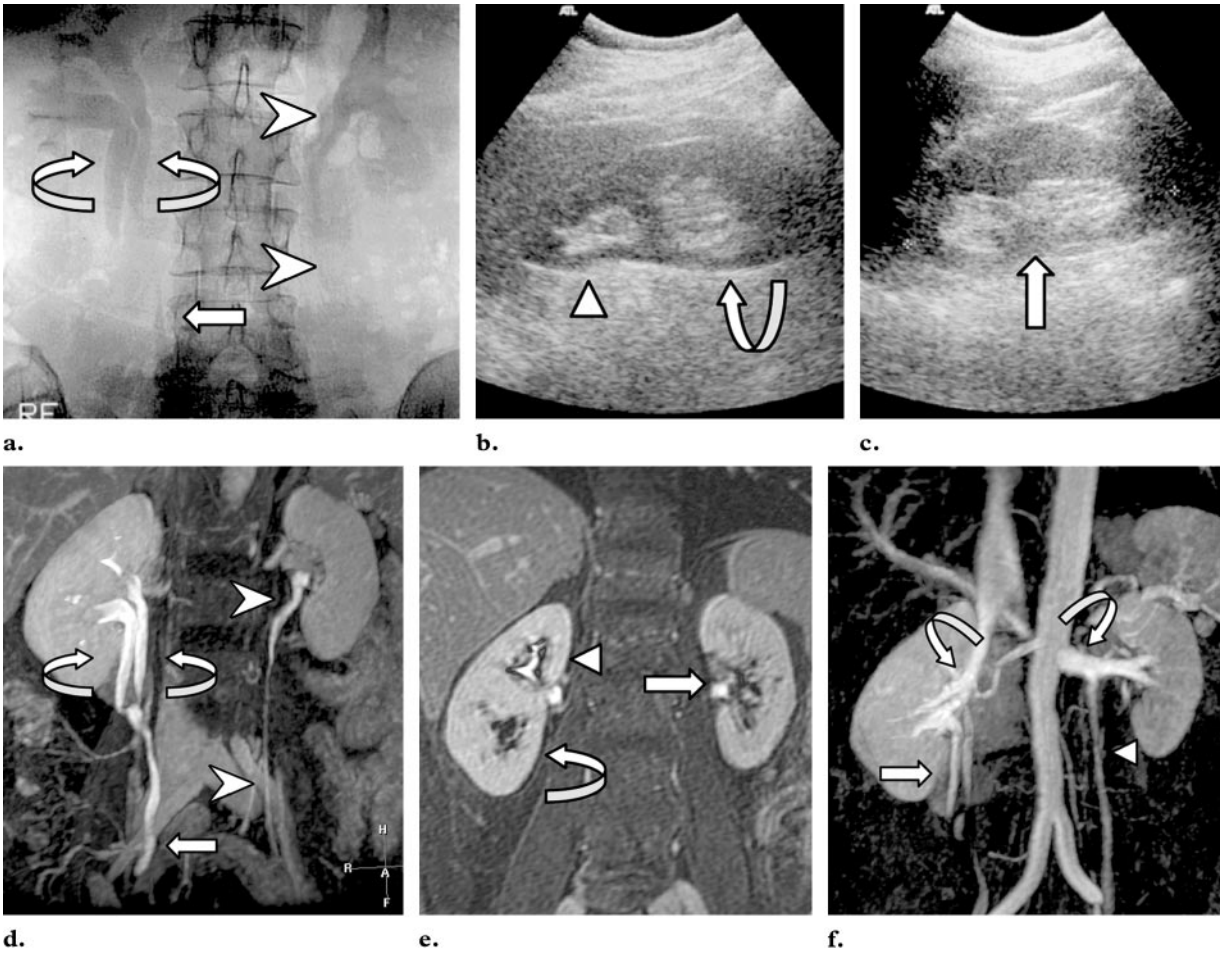

Figure 10. Intravenous urographic, US, and MR imaging findings in duplication of the right renal collecting system. **(a)** Intravenous urogram shows duplication of the right renal pelvis and proximal ureter (curved arrows). The distal right ureter is just visible as a single structure (straight arrow). The left collecting system is normal (arrowheads). **(b)** Longitudinal US image of the right kidney shows a parenchymal bridge that separates the medulla within a smaller upper pole (arrowhead) and larger lower pole (arrow), findings compatible with a duplicated collecting system. **(c)** Longitudinal US image of the left kidney shows a normal-sized kidney with a normal medullary region (arrow). **(d)** Coronal targeted MIP image from the MR angiography data set of the venous phase shows more clearly the duplication of the proximal collecting system on the right side (curved arrows) with a single ureter distally (straight arrow). The left collecting system is normal (arrowheads). **(e)** Coronal targeted MIP image of the venous phase obtained at the level of the medulla of the kidneys shows the relatively dysplastic upper pole (arrowhead) and larger lower pole (curved arrow) on the right side, whereas the left kidney is normal (straight arrow). **(f)** Coronal full MIP image of the arterial phase with some venous enhancement shows the relationship of the renal veins (curved arrows) to the gonadal vein on the left side (arrowhead) and the duplicated collecting system on the right (straight arrow).

lumber, adrenal, and gonadal veins (Fig 10f). These veins empty into the left renal vein in about 75%, 100%, and 100% of individuals, respectively (4). Recently, Pozniak and colleagues (4) described the anatomic variations of the renal vessels in an article based on their experience with CT angiography.

Similarly to vascular anatomic variations, duplication of the upper urinary tract, particularly duplication of the abdominal parts of the ureter and renal pelvis, is common (11). These abnormalities result from the division of the ureteric bud (11). The extent of ureteral duplication depends on how complete the division of the diverticulum is (11). Incomplete division of the diverticulum results in a divided kidney with a bifid ureter (Fig 10).

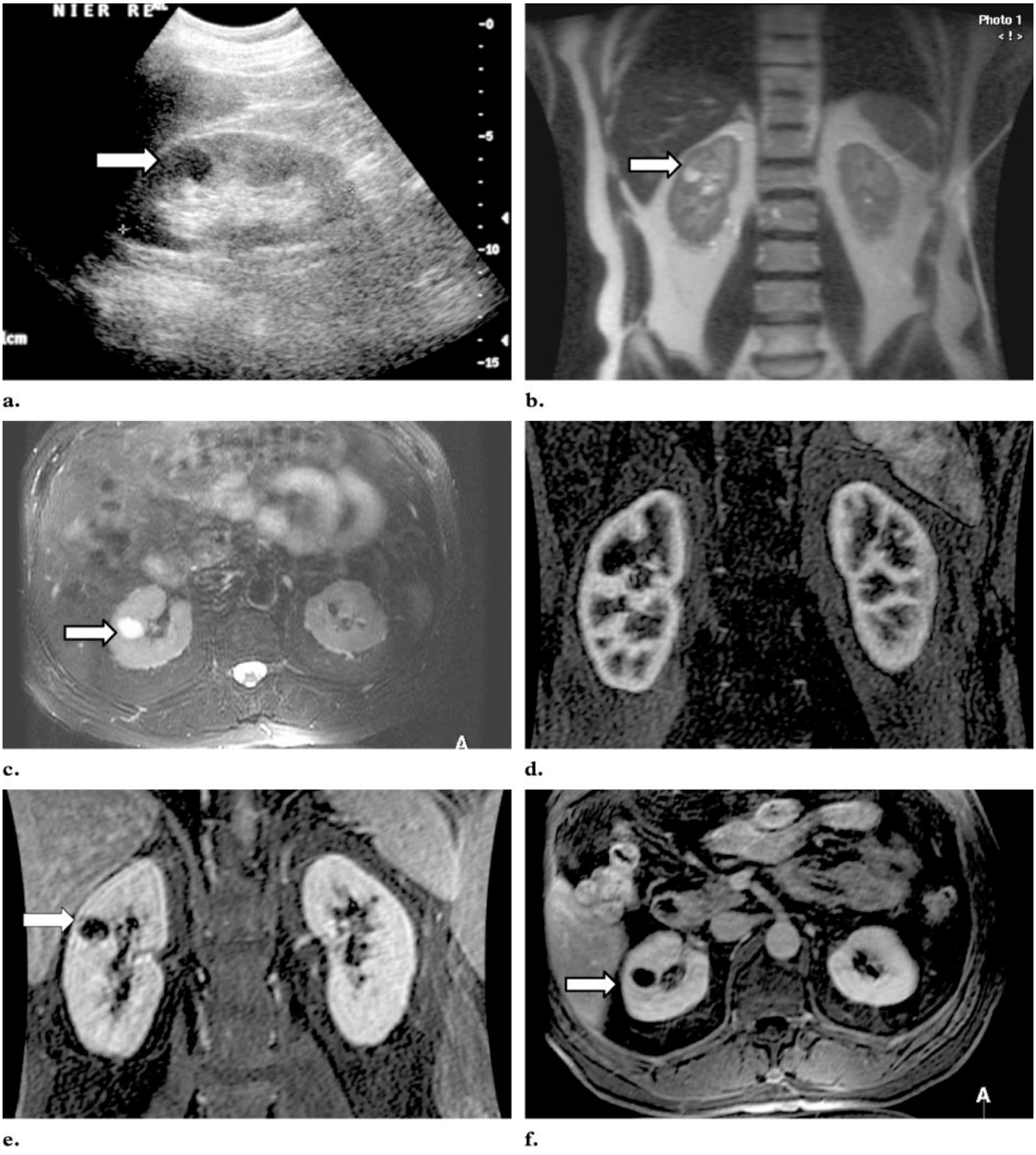

Figure 11. Renal cyst at US, MR imaging, and MR angiography. **(a)** Longitudinal US image shows the right kidney, which has a small cyst in the upper pole (arrow). **(b)** Coronal single-shot fast SE image shows the cyst as a hyperintense, sharply marginated lesion (arrow). **(c)** Axial T2-weighted fast SE image obtained with fat saturation also shows the cyst (arrow). **(d)** Coronal source image from the MR angiography data set does not show a well-circumscribed lesion. **(e)** Coronal source image from the MR venography data set shows the cyst clearly (arrow). **(f)** Axial delayed gadolinium-enhanced 3D fast GRE image obtained with fat saturation shows the cyst as a nonenhancing, sharply marginated structure (arrow). This sequence allows exclusion of any lesion with slowly enhancing solid components.

Renal parenchymal abnormalities in living donors are not often encountered. In our opinion, the best sequences for excluding such abnormalities are the T2-weighted half-Fourier single-shot turbo SE, fast SE with fat saturation, and delayed gadolinium-enhanced T1-weighted GRE sequences (Fig 11). The MR angiography and MR venography data sets in our MR imaging protocol are not always suitable for this purpose because

these sequences are optimized for imaging the vessels and may obscure parenchymal abnormalities due to insufficient anatomic coverage or fold-over artifacts.

Discussion and Conclusions

This article discusses and illustrates a number of points related to imaging of potential kidney donors. First, the vascular anatomy of living kidney donors may be complex and is closely interrelated with other anatomic structures. Second, MR imaging is capable of demonstrating the anatomy of living kidney donors as well as the interrelated anatomic structures on high-quality images. Third, this article illustrates the usefulness of a comprehensive but simple approach with MR imaging for assessment of living kidney donors. Finally, a number of different display methods are helpful for conveying the message to the surgeon (12).

The accuracy of MR angiography is comparable with that of CT angiography (7). Both MR angiography and CT angiography are highly accurate for assessment of the main renal vessels and the larger accessory renal vessels (7). Accuracy rates of higher than 90% have been reported (4,5). In many institutions, CT angiography has replaced DSA as the modality of choice in the work-up of living kidney donors (9,10,13). However, living kidney donors are healthy; therefore, we prefer a comprehensive work-up with MR imaging because of the lack of radiation and nephrotoxic contrast agents. Currently, a more systematic assessment of MR imaging data from living kidney donors in our hospital is being performed. The preliminary results indicate that the information provided by MR imaging is helpful in clinical decision making, for instance, when making a choice between the right and left kidneys (M.G.M.H., unpublished data, 2001). In addition, visualization of the exact course and the relationship of the arteries and veins improves the surgeon's confidence during the harvesting procedure (M.G.M.H., unpublished data, 2001). This may help further reduce the operation time and the risk of complications.

Our MR imaging protocol is designed to show the arterial system, venous system, and collecting system of the kidneys. However, in many centers, DSA, CT angiography, and MR angiography are mainly focused on the arterial vessels. Conventional subtraction venography or CT venography is not often performed as a separate dedicated study to visualize the exact venous anatomy in the work-up of living kidney donors (9,13). Time-of-flight and phase-contrast MR venography, which do not require intravenous paramagnetic contrast media such as gadopentetate dimeglumine, have evolved into reliable and clinically accepted methods for assessment of the deep venous system (3). Because of the presence of slow flow and tortuous venous anatomy, in our experience these techniques are of limited use in the work-up of living kidney donors. Furthermore, the examinations can be time-consuming. Therefore, we prefer 3D gadolinium-enhanced MR venography for assessment of the venous system of living kidney donors.

The superiority of MR imaging is due to differences in techniques of data acquisition and contrast medium administration, in addition to the inherently greater tissue contrast of MR imaging (14). First, in most centers, dynamic gadolinium-enhanced MR imaging is currently performed with multisection two-dimensional or 3D GRE sequences. Such sequences have several intrinsic features that make them superior to CT. One of the advantages is that the central k-space profiles, which determine the image contrast in all individual sections, are acquired in less than half the total duration of one breath-hold sequence (5–10 seconds). Second, fast MR imaging sequences allow the use of timing bolus or automated contrast detection techniques to determine the contrast material arrival time within the aorta, without any concerns about radiation hazards. Finally, in MR imaging, a smaller amount of contrast medium (28 mL of gadolinium contrast medium) is injected. This allows a short injection time with a compact bolus (3). This facilitates the imaging of truly distinct arterial and venous phases. An additional value of the gadolinium-enhanced MR venography sequence in our protocol is that it is also useful as an MR urography sequence.

There are a number of limitations of MR imaging. First, renal stones, especially if present within the renal parenchyma, would not be visualized with the currently available MR imaging sequences. Usually, renal calculi larger than 5 mm or multiple calculi have consequences for the harvesting procedure (4). To rule out such calculi, plain abdominal radiography, US, or even plain CT may still be needed. At some institutions, the

presence of multiple small calculi may be one of the exclusion criteria for donation. Plain radiography, particularly when performed with an unprepped intestine, may not be sensitive enough for detecting these small calculi. Unenhanced CT is a sensitive modality for detecting calculi. Second, the 3D GRE nature of the MR angiography sequence makes it sensitive to motion, such as pulsations within the vessels and field inhomogeneities. These factors may degrade image quality in some patients. In such patients, we often perform an additional DSA or CT angiography study to evaluate the renal vasculature. At our hospital, intravenous urography is not part of the imaging work-up of renal donors. Third, any contraindications to MR imaging, such as a pacemaker or vascular clips, or claustrophobia would prevent use of MR imaging in the work-up of living kidney donors. Fourth, although MR imaging is highly accurate for detection of renal vascular abnormalities, such as renal artery stenosis (3), the detection of very subtle disease, including atherosclerotic disease and fibromuscular dysplasia, is less accurate. Furthermore, the availability of MR imaging in many countries is lower than that of CT. Finally, although MR angiography may seem an expensive modality for investigating living kidney donors, a cost-effectiveness analysis of MR imaging compared with other strategies performed at our institution demonstrated that it is cost-effective (15).

Despite these limitations, MR imaging, including various T1-weighted, T2-weighted, MR angiography, and MR venography sequences, has the potential to become the modality of choice in the work-up of living kidney donors (5). The source images allow reconstruction of MIP images and reformatted images in any desired plane and facilitate understanding of the complex nature of the renal anatomy.

References

1. Schaffer D, Sahyoun AI, Madras PN, et al. Two hundred and one consecutive living-donor nephrectomies. Arch Surg 1998; 133:426–431.
2. Lind MY, IJzermans JNM, Bonjer HJ. Open vs laparoscopic donor nephrectomy in renal transplantation. BJU Int 2002; 89:162–168.
3. Prince MR, Grist TM, Debatin JF. 3D contrast MR angiography. 2nd ed. Berlin, Germany: Springer-Verlag, 1999; 163–171.
4. Pozniak MA, Balison DJ, Lee FT Jr, et al. CT angiography of potential renal transplant donors. RadioGraphics 1998; 18:565–587.
5. Low RN, Martinez AG, Steinberg SM, et al. Potential renal transplant donors: evaluation with gadolinium-enhanced MR angiography and MR urography. Radiology 1998; 207:165–172.
6. Nelson HA, Gilfeather M, Holman JM, et al. Gadolinium-enhanced breathhold three-dimensional time-of-flight renal MR angiography in the evaluation of potential renal donors. AJR Am J Roentgenol 1997; 168:1569–1573.
7. Halpern EJ, Mitchell DG, Wechsler RJ, Outwater EK, Moritz MJ, Wilson GA. Preoperative evaluation of living renal donors: comparison of CT angiography and MR angiography. Radiology 2000; 216:434–439.
8. Agildere AM, Tutar NU, Demirag A, et al. Renal magnetic resonance angiography with Gd-DTPA in living renal transplant donors. Transplant Proc 1999; 31:3317–3319.
9. Del Pizzo JJ, Sklar GN, You-Cheong JW, et al. Helical computerized tomography arteriography for evaluation of live renal donors undergoing laparoscopic nephrectomy. J Urol 1999; 162:31–34.
10. Kim TS, Chung JW, Park JH, et al. Renal artery evaluation: comparison of spiral CT angiography to intra-arterial DSA. J Vasc Interv Radiol 1998; 9:553–559.
11. Moore KL. The developing human. 3rd ed. Philadelphia, Pa: Saunders, 1982; 265.
12. Pace ME, Krebs TL, Wong-You-Cheong JJ, et al. Comparison of three display methods for evaluating CT angiography data for the vascular assessment of renal donors. J Digit Imaging 1998; 11: 145–148.
13. Shokeir AA, el-Daisty TA, Nabeeh A, et al. Digital subtraction angiography in potential live-kidney donors: a study of 1000 cases. Abdom Imaging 1994; 19:461–465.
14. Schoenberg SO, Prince MR, Knopp MV, Allenberg JR. Renal MR angiography. Magn Reson Imaging Clin N Am 1998; 6:351–370.
15. Liem YS, Kock MCJM, IJzermans JNM, Weimar W, Visser K, Hunink MGM. Living renal donors: optimizing the imaging strategy—decision- and cost-effectiveness analysis. Radiology 2003; 226: 53–62.

This article meets the criteria for 1.0 credit hour in category 1 of the AMA Physician's Recognition Award. To obtain credit, see accompanying test at http://www.rsna.org/education/rg_cme.html.